Gabor Lens Beam Experiments

Toby Nonnenmacher, Chung Lim Cheung, Juergen Pozimski

July 16, 2020

Abstract

Results of beam experiments will be presented and compared with results from particle tracking simulations performed using GPT - by Juergen

I. Introduction

The strong focussing forces that in theory can be provided for low and medium energy ion beams by space charge lenses of the Gabor type [1] [7] make them excellently suited to be used to capture particle beams accelerated by laser interaction. In theory this type of lens system offers an increase in focussing strength by more than a factor of 40 compared with solenoid capture. It has been shown by simulation results that even the capture of proton beams at full proton cancer therapy energies (250 MeV) is concievable [5]. To demonstrate the advantages of space charge lenses for the capture of ion beams, an experimental program was started at Imperial College London with the aim of demonstrating particle capture and beam formation at energies capable of performing in vitro RBE experiments (5-15 MeV protons).

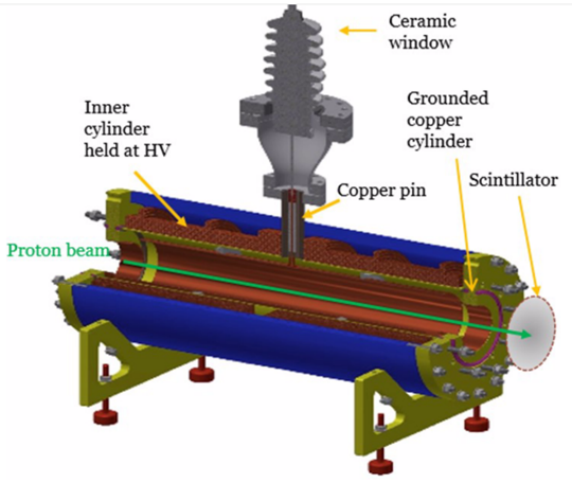

Figure 1: *Internal structure of the IC Gabor lens including the electrodes. The direction of beam test a particle beam is shown penetrating the lens and impinging a scintillator screen.*

II. The Gabor Lens

While the experimental determination of the optical properties of the Gabor lenses built and operated in Frankfurt [3] did show a relatively good agreement between the predictions of the space charge density distribution gained by numerical codes and the predicted beam transport properties of the lenses compared with the experimentally gained results. Especially the strong variation of the space charge density with time, which is the only possible cause for the observed beam transport properties for the lens that was built and tested at Imperial [9] for use as an ion capture device following an initial ion source and laser acceleration stage for medical applications in cancer therapy.

A schematic of the Imperial college Gabor lens is shown in Figure 1. The lens has a total length of 540 mm and makes use of a high electron density of around $5 \times 10^{-7}\ Cm^{-3}$. The inner and outer diameter of the central electrode shown in the figure are 66 mm and 89 mm respectively. Plasma in the lens is produced by increasing the high voltage through the lens, and the current in the magnetic coils reaching a maximum field of approximately 55 mT for a magnetic field of $45A$. The pattern of magnetic

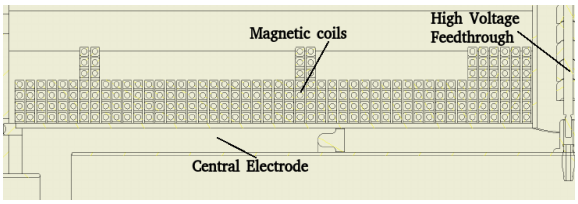

Figure 2: *Schematic drawing of the top left quarter of the lens. The pattern of magnetic coils above the central electrode is shown.*

Figure 3: *The segmented detector used for initial measurements of plasma in the Gabor Lens. The detector is divided in to 16 sections of equal area.*

coils is shown in Figure 2. Measurements of the plasma in the lens were made using the Medusa detector shown in Figure 3. This detector is divided into 16 equal sections with of area 122.5 mm^2.

III. Applications

Laser based accelerators producing ion, proton, and electron beams are increasingly finding uses as an alternative to conventional accelerators, such as synchrotrons and cyclotrons. A major advantage of laser based accelerators is their relative size, being much smaller and cheaper than a synchrotron or cyclotron at equivalent energies, resulting in possible cost-savings. The reduction in size stems from the wavelength of the EM wave being approximately 10^6 times shorter than that of a conventional accelerator [4]. The Gabor lens is the ideal partner of laser-accelerated beams due its ability to reach high focusing with a low magnetic field compared with conventional solutions. For example, for a 25 MeV proton beam, in order to achieve a focal length of 1 m the required field is 0.06 T for a Gabor lens of 0.3 m, in contrast with 2.6 T for a solenoid with the same effective length. This is particularly important when beams are produced with a large divergence angle [9]. Moreover, its compactness and relatively low price are key if it is installed in particle beam therapy facilities.

While laser based systems cannot yet access energies available using conventional accelerators, laser technology is improving. In the last 10 years, laser driven accelerators have been shown to be capable of producing beams of energy 60 MeV, with a predicted increase of at least a factor of 5 to 10 [6]. This increase is a realistic prospect, because, in increasing the attainable energy, the effort of providing the initial 30 MeV was much greater than in increasing the beam energy from 30 to 60 MeV. A strong possible future application of a beam accelerated by a laser and focused by a Gabor lens would be in proton beam therapy [5].

One application of Gabor lenses within reach of current available technology is in radio nuclide production. Available laser systems can handle proton energy exceeding 25 MeV, which is sufficient for production of Tc^{99} from Mo^{99} in combination with focusing from a Gabor Lens lattice [10]. Other applications of the Gabor Lens are also conceivable.

IV. Initial Studies

Measurements of the contents of the lens were made using the Medusa detector in 3 different plasma regions:

- Plasma off - high voltage and current through coils below the threshold for plasma to be produced
- Stable Plasma - plasma produced with high voltage below 25 kV and current through magnetic coils below 27 A

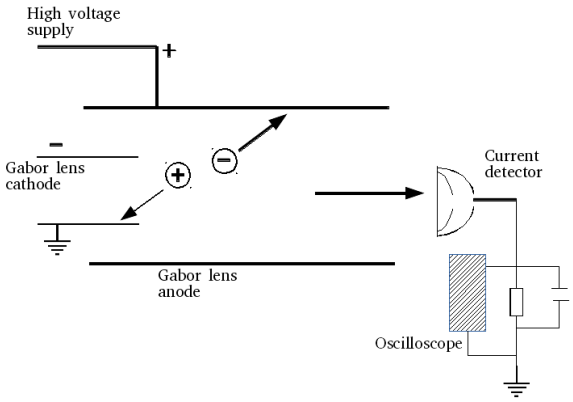

Figure 4: *Schematic of the Gabor lens, current detector, and oscilloscope/ The high voltage supply maintains the drop across the electrodes. Expelled ions hit the detector, and the current signal is converted to a voltage output signal in the oscilloscope.*

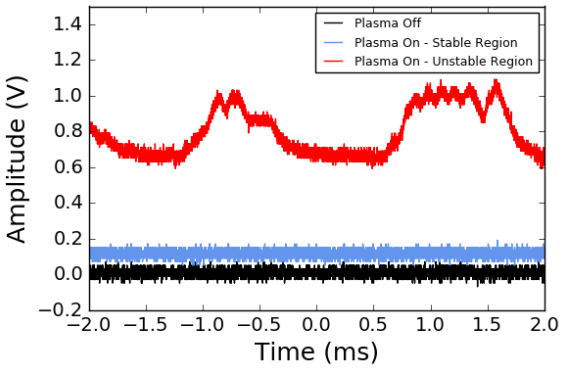

Figure 5: *Amplitude of signal from the Medusa detector in three regions: plasma off, plasma on, and plasma on in unstable region. The time range is given 0.0004 s, and the time resolution of the measurement is 4x10*-7 s. The voltage range is 0.5 V with a resolution of 0.01 V*

	Mean	**Standard Deviation**
Plasma Off	0.0082∼V	0.0190∼V
Plasma On	0.1143∼V	0.0199∼V
Plasma Unstable	0.7965∼V	0.1327∼V

Table 1: *Mean and Standard Deviation values for Plasma Off, On, and Unstable regions shown in figure 5*

- Unstable Plasma - plasma produced with higher magnetic field causing considerable sparking

The amplitude results of these measurements are shown in Figure 5 and frequency results of the fourier transform of these amplitudes are given in Figure 6. The frequencies chosen for the measurement were those below 2.5 MHz as previous bode plotting indicated frequencies below 1 MHz are not filtered out. As the frequency profile contains one primary peak, a uniform window was chosen for the fourier transform.

The mean and standard deviation in the different plasma regions are contained in table 1. The mean increases slightly, when the plasma

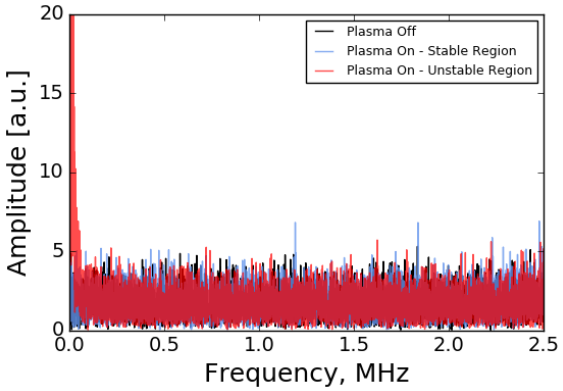

Figure 6: *Fourier transform of signal from the Medusa detector in three regions: plasma off, plasma on, and plasma on in unstable region. The number of sammples for this measurement was 10000, with a frequency range of 2.5 MHz and resolution of 500 Hz*

is switched on, while the standard deviation remains largely unchanged. As the current applied through the coils becomes too large, and the unstable region is reached, the mean and standard deviation rise and a large amount of noise is seen.

This is seen in figure 6, where the level of noise is very similar with the plasma off and on, and only increases appreciably upon reaching the unstable region. In this region, the low frequency noise is increased significantly, while the high frequency noise remains largely unchanged.

V. Beam Test Setup

The beam test took place at the Ion Beam Facility at the University of Surrey in October 2017. The Gabor Lens was operated with a pencil beam of 1.4 MeV protons over the course of two days.

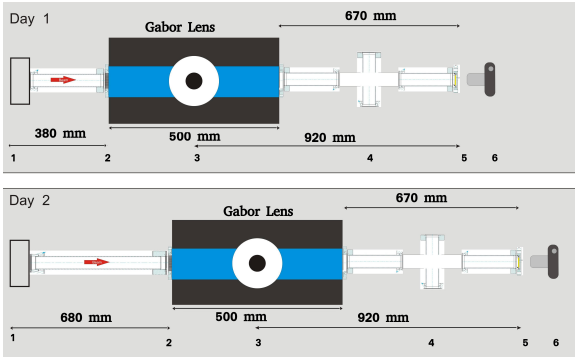

Figure 7: *Schematics of the day 1 beam test setup, Setup 1 (top) and the day 2 beam test setup, Setup 2 (bottom). The setup includes the Gabor lens, aperture, and beam pipes*

Two different configurations were used during the beam test, as shown in Figure 7. The Gabor lens was placed approximately 380 mm and 680 mm from the the beam entrance on the first and second day of beam operation respectively. The increased distance from the beam line on the second day allowed for a broader image of the beam to be observed. Henceforth, the shorter Day 1 setup is referred to as Setup 1 and the longer Day 2 setup as Setup 2.

Between the initial beam pipe, and the lens, an aperture was placed, shown in Figure 8. This

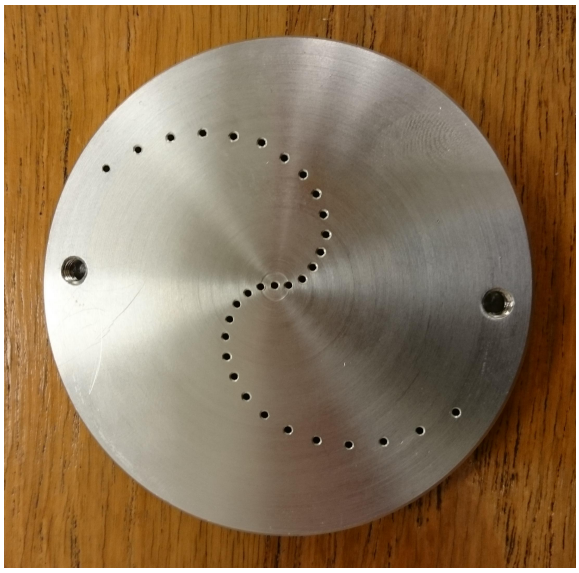

Figure 8: *Photograph of the aperture placed in the beamline upstream of the Gabor Lens. 30 holes of 2 mm width are drilled in a symmetrical pattern around one further hole on the axis. The surrounding holes are pitched at an angle of 20°*

aperture split the incoming pencil beam into many individual beamlets of smaller diameter. The rotational pattern of aperture holes was designed to minimise the overlap of the outgoing beamlets under a rotationally symmetric force applied at the beam axis. This is effective, even for quadrupole focusing. In both configurations, following focusing in the lens, the beamlets travelled through another 670 mm beam pipe before impinging on a phosphor screen, shown in figure 9. While the distance between the Gabor Lens and Phosphor screen was known precisely, it was not possible to measure the distance from the final quadrupole to the lens with the same precision. The phosphor screen used was a P43 phosphor surface on an aluminized pyrex substrate, with an effective area of diameter 44.9 mm. The screen was 10-15 μm thick.

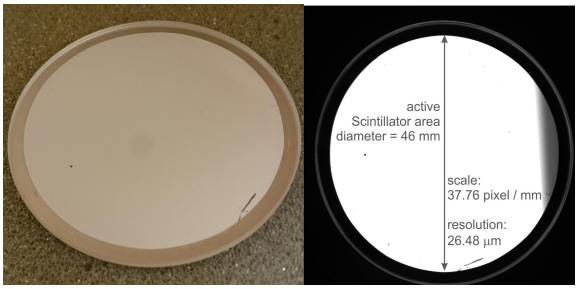

Figure 9: *Photograph and schematic of the phosphor screen used for imaging the beam. The screen was composed of a P43 phosphor surface on a substrate of aluminized pyrex, and the scale and resolution of the screen are shown on the schematic.*

VI. Analysis

Figure 10 shows a comparison between lens behaviour in the initial studies and during the beam test. Variation of the voltage readings of the Medusa detector described in section II with changing current through the lens coils was measured. The measurements of the beam spots made during the beam test with the lens on were in the range 18-32 A. In this region, the shape of the curves is very similar, demonstrating that the lens was being operated in the low noise, stable plasma region.

Figure 11 shows camera images of the beam in the Setup 1 and 2 configurations of the beam test setup described in section V, with the lens off. The distinct beam spots were produced by passing the beam through the aperture. The longer Setup 2 configuration allowed for more of the aperture holes to be seen in a single camera image. The central, on axis spot (2nd from the right in both setups) does not lie at the centre of the screen, implying that the beam axis and lens magnetic axis were not aligned.

Figure 12 shows camera images of the beam in the Setup 2 configuration with the lens on at 20 kV. The magnetic current was increased and the formation of rings as a result of increased focusing was observed. The original pencil beams were focused into ring shapes with lower intensity towards the centre. The eccentricity of these increased with increasing radial distance from the beam axis.

To see this effect better, figure 13 shows a 3D plot of these beam spots, from a birds eye view along the beam axis. The beam spots are clearly visible against the low background, and are not uniform spots, but rather have a ring structure. The rings are themselves not consistent in amplitude, but rather contain some modulation. This implies the lens plasma was not uniform but rather hollow close to the lens axis, causing the plasma to oscillate in its rotation. Similar behaviour was previously observed in [2]. However, in contrast to the results in [2], in which only a single circular structure was observed, the measurements described here reveal a cylindrical structure produced for every beamlet. Additionally, one ring per beamlet was previously observed in [8], but the additional detail of the measurements shown demonstrate that these beamlets become more elliptical with increase in radius.

A comparison of the effects of electric field only and magnetic field only in the lens is shown in figure 14. This plot presents data from Setup 1, in which the 3 spots are those shown in figure 11, with the rightmost point corresponding to the beam axis centre. Squares and Circles represent variation in current through the magnetic coils only, in simulation and data respectively, with no applied high voltage. Crosses represent variation in high voltage (and therefore electric field) with no current through the magnetic coils. As expected from theoretical consideration, applying only electric potential does not influence the particle transport to a degree comparable with variation from change in magnetic field. Comparison between magnetic field only data and calculated influence of particle transport due to magnetic field shows good agreement in direction as well as magnitude. This is true for all three of the observed pencil beamlets. The small variation around the pencil beam on the beam axis indicates that the beam axis, aperture axis, and lens axis were not identical.

Figure 15 shows the variation in X and Y position of the three beam spot centres in Setup 1, under the effects of both applied magnetic field

and high voltage. In this case, the high voltage is held at 15 kV, while the current through the magnetic coils is varied from 0 to 32 A. An approximately linear increase with magnetic field is observed. Given the expectation that the lens plasma density should increase as the square of the field, this implies an alternative limiting factor: in addition to the force producing circular motion in the lens, there is a force that is constant in time causing an off centre drift.

The variation in X and Y diameter of the six beam spots from Setup 2 is given in Figure 16: with a constant applied voltage of 15 kV, the variation in spot diameter with magnetic field is shown. A non-linear increase in spot size with change in magnetic fields is observed, with the rate of increase in diameter getting larger at high magnetic fields. This gives an indication of higher order effects on the increases in diameter. The increase in plasma density with magnetic field is larger than linear. That the points remain within the lines shown, implies that the ratio between X and Y stays the same for a given spot. The ratio variation being solely dependent on initial position of spot, indicates that this effect is caused by the plasma density distribution in the transverse plane.

Figure 17 shows the change in XY ratio of the six beam spots from Setup 2 with variation in magnetic field. The forces in X and Y change to different extents, with an increased difference at greater distances from the beam axis. At those points farther from the beam centre, the force in X is bigger than in Y, indicating that the centre of the lens has a low plasma density, while further from the axis of the lens, the plasma density increases with radius. Additionally, there is some perturbation in the motion of the plasma with a time dependence. Together figures 14 to 17 describe the shape of the plasma within the lens: A position dependent plasma is indicated, with a hollow centre, and a density increasing with radius, rotating around the lens centre.

VII. Conclusions

VIII. Outlook

IX. Acknowledgements

References

[1] Dennis Gabor. "A space-charge lens for the focusing of ion beams". In: *Nature* 160.4055 (1947), p. 89.

[2] U. Neuner et al. "Shaping of Intense Ion Beams into Hollow Cylindrical Form". In: *Phys. Rev. Lett.* 85 (21 Nov. 2000), pp. 4518–4521. DOI: 10.1103/PhysRevLett.85.4518. URL: https://link.aps.org/doi/10.1103/PhysRevLett.85.4518.

[3] J Pozimski and O Meusel. "Space charge lenses for particle beams". In: *Review of scientific instruments* 76.6 (2005), p. 063308.

[4] AA Goncharov et al. "Electrostatic plasma lens for focusing negatively charged particle beams". In: *Review of Scientific Instruments* 83.2 (2012), 02B723.

[5] J. Pozimski and M. Aslaninejad. "Gabor lenses for capture and energy selection of laser driven ion beams in cancer treatment". In: *Laser and Particle Beams* 31.4 (2013), pp. 723–733. DOI: 10.1017/S0263034613000761.

[6] J Pozimski and M Aslaninejad. "Gabor lenses for capture and energy selection of laser driven ion beams in cancer treatment". In: *Laser and Particle Beams* 31.4 (2013), pp. 723–733.

[7] Kathrin Schulte et al. "Gabor Lens Performance Studies at the GSI High Current Test Injector". In: *Proceedings, 4th International Particle Accelerator Conference (IPAC 2013): Shanghai, China, May 12-17, 2013*. 2013, THPWO021. URL: http://JACoW.org/IPAC2013/papers/thpwo021.pdf.

[8] Piero Antonio Posocco et al. “First Test of The Imperial College Gabor (Plasma) Lens prototype at the Surrey Ion Beam centre”. In: *Proceedings, 7th International Particle Accelerator Conference (IPAC 2016): Busan, Korea, May 8-13, 2016*. 2016, TUPMY024. DOI: 10.18429/JACoW-IPAC2016-TUPMY024.

[9] Jürgen Pozimski, Morteza Aslaninejad, and Piero Antonio Posocco. “Advanced Gabor Lens Lattice for Laser Driven Hadron Therapy and Other Applications”. In: *Proceedings, 7th International Particle Accelerator Conference (IPAC 2016): Busan, Korea, May 8-13, 2016*. 2016, TUPMY023. DOI: 10.18429/JACoW-IPAC2016-TUPMY023.

[10] Jürgen Pozimski, Morteza Aslaninejad, and Piero Antonio Posocco. “Advanced Gabor Lens Lattice for Laser Driven Hadron Therapy and Other Applications”. In: (2016).

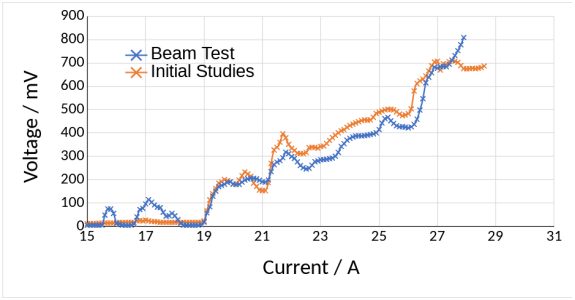

Figure 10: *Comparison of the plasma regime at the beam test in Surrey with the previous lab plasma conditions. During the beam test, the lens gas pressure was 10% higher, and measurements were made in the Current region of 18-32A*

Figure 11: *Observed camera image of the 3 beam spots beyond the aperture in the Setup 1 configuration, left, and with 6 beam spots beyond the aperture in the Setup 2 configuration, right. Both images were taken with the lens off*

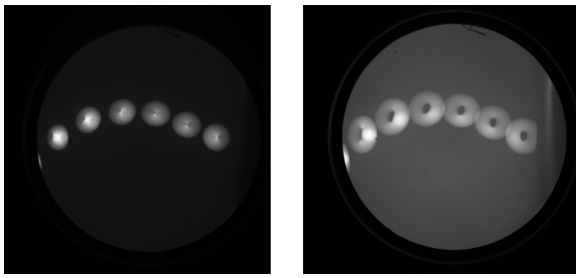

Figure 12: *Observed camera image of the 6 beam spots beyond the aperture in the Setup 2 configuration with the lens on at a current through the coils of 28 A, left and 33 A, right. Both images were taken with a lens voltage of 20kV. An additional spot is visible on the left hand side, as the lens focusing is increased*

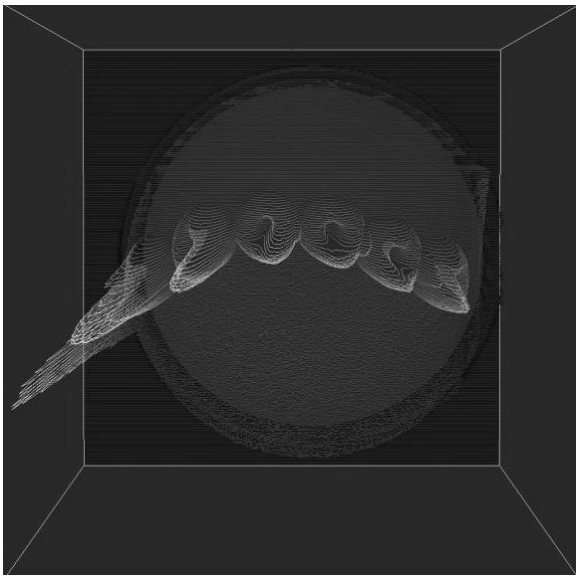

Figure 13: *3D plot of the scintillator measurement of the 6 beam spots in the Setup 2 configuration, with the lens on. The image is shown looking down along the beam axis*

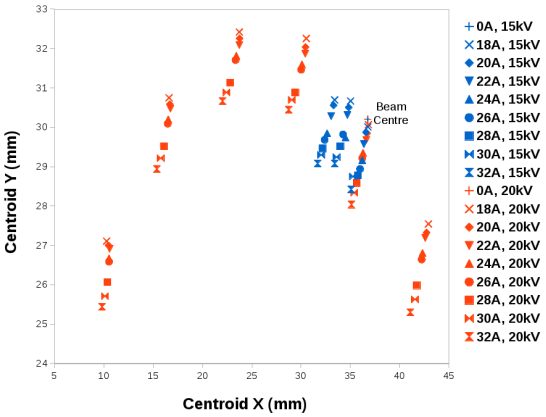

Figure 15: *Plot showing Centroid X vs Centroid Y for the 3 spot data with increasing magnetic field strength*

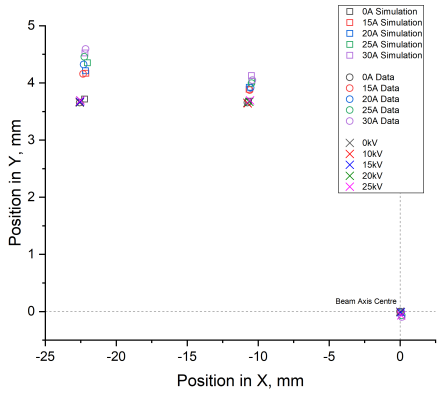

Figure 14: *Position of the centre of the 3 beam spots for varying magnetic fields and high voltages. Data is represented by circles and crosses, while simulated data is represented by squares*

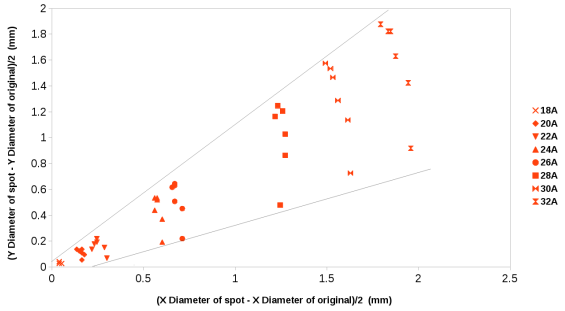

Figure 16: *Plot showing variation in X and Y diameter of the 6 spot data with increasing magnetic field strength, compared with no magnetic field*

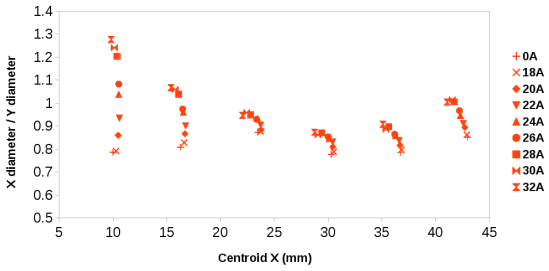

Figure 17: *Plot showing ratio of X diameter to Y diameter for beam spots in the 6 spot data with increasing magnetic field strength*